*Forest Chemicals Revew*
*www.forestchemicalsreview.com*
*ISSN: 1520-0191*
*July-August 2021 Page No. 1469-1482*
*Article History: Received: 12 May 2021 Revised: 25 June 2021 Accepted: 22 July 2021 Publication: 31 August 2021*

# Research on Multi-Scale High-Fidelity Digital Model and Reduced-Order Model for Digital Twin Modeling of Composite Structures

**Jiale Zuo [1], Dong Li[2*], Ling Zhou [1], Cun Zhang [3], Huicong Wang[4]**

[1]Nanchang Hangkong University, School of Aircraft Engineering, Nanchang, Jiangxi, 330063, People's Republic of China

[2]Hebei Jiaotong Vocational and Technical College, Center for Quality Management, Shijiazhuang, Hebei, 050035, People's Republic of China

[3]Shijiazhuang Tiedao University, State Key Laboratory of Mechanical Behavior and System Safety of Traffic Engineering Structures, Shijiazhuang, Hebei, 050043, People's Republic of China

[4]Hebei Jiaotong Vocational and Technical College, Department of Road and Bridge Engineering, Shijiazhuang, Hebei, 050091, People's Republic of China

*Corresponding Author.

***Abstract:***

The research purpose of this paper is to establish a multi-scale high-fidelity digital model and a reduced-order model for digital twin of composite structures. Firstly, a high-fidelity digital model is established for the composite structure using micro-meso-macro multi-scale method to accurately describe the composite structure. Then, in order to meet the real-time needs of digital twin, the reduced-order model is studied by using three training algorithms for comparative study: Bayesian Regularization (B-R), Levenberg-Marquardt (L-M), and Scaled Conjugate Gradient (SCG). B-R training algorithm with smaller error is chosen to establish a neural network reduced-order model. Finally, with the multi-scale high-fidelity digital model as a reference, the maximum error of the established reduced-order model is 5.64%, which can meet the needs for multi-scale digital twin modeling of composite structures.

***Keywords****: Composite structure, High-fidelity digital model, Reduced-order model, Multi-scale modeling, Neural network.*

## I. INTRODUCTION

Composites are widely used in aviation, aerospace, shipbuilding, machinery fields [1]. The mechanical properties and failure mechanism of composites are not only related to macroscopic properties but also closely related to microscopic parameters like component properties,

*Forest Chemicals Revew*
*www.forestchemicalsreview.com*
*ISSN: 1520-0191*
*July-August 2021 Page No. 1469-1482*
*Article History: Received: 12 May 2021 Revised: 25 June 2021 Accepted: 22 July 2021 Publication: 31 August 2021*

distribution, interface. Hence, the composite failure state and failure mode are more complicated than metal materials. As a disruptive frontier technology, digital twin technology is of great engineering application value in the prediction of damage and fatigue behavior of composite structures. The key technology in digital twin of composite structures lies in online deployment of multi-scale high-fidelity digital modeling and its reduced-order models. Therefore, it is necessary to establish a multi-scale composite model to accurately express the composite structure [2], and study reduced-order model to meet real-time requirements.

In 2011, the U.S. Air Force Laboratory proposed the concept of Airframe Digital Twin and applied the digital twin technology to the life management of aircraft structures [3]. Lai and Song et al. established a crane digital twin model for real-time analysis based on SPI-DA, including analysis model, theoretical model and artificial intelligence model [4]. Botz et al. used historical data and finite element data to establish a reduced-order model for the nonlinear structure of wind turbines, which provided a basis for the establishment of digital twin model [5]. Saboktakin et al. took two-dimensional braided composite as the research object, established a multi-scale high-fidelity digital model to simulate tensile progressive damage, and verified accuracy of the method through experiments [6]. By combining data-driven technology, Han et al. established a reduced-order model based on the establishment of microscopic and mesoscopic models to predict the macroscopic properties of composite structures [7]. Wu et al. carried out a multi-scale analysis of braided composites, using microscopic parameters as the input parameters of the reduced-order model (ROM) for learning and training, and used the reduced-order model for nonlinear analysis of the braided composites [8].

The above-mentioned research objects for digital twin are mostly metal material structures, and there are few researches on digital twin for composite structures. Also, there are few studies on multi-scale high-fidelity digital models and reduced-order models that support the digital twin modeling of composite structures. Therefore, this paper takes composite structure as the research object and establishes a multi-scale high-fidelity digital model and a reduced-order model that can be used for digital twin of composite structure to provide a basis for the establishment of digital twin model for composite structures.

## II. EXAMPLE VERIFICATION OF MULTI-SCALE MODELING AND REDUCED-ORDER MODEL

### 2.1 Multi-scale Modeling

#### 2.1.1 Micro and Meso-scale modeling

Microstructure refers to the structure of a material at a micro-scale. Different material

*Forest Chemicals Revew*
*www.forestchemicalsreview.com*
*ISSN: 1520-0191*
*July-August 2021 Page No. 1469-1482*
*Article History: Received: 12 May 2021 Revised: 25 June 2021 Accepted: 22 July 2021 Publication: 31 August 2021*

microstructures will cause huge differences in material mechanical properties. Fabric composites have different constituents at the meso-scale and micro-scale levels, and changes in material structure on these two scales will cause changes in mechanical properties of the materials. In multi-scale modeling, micro-scale modeling is first performed to establish the model of single fiber and matrix. Mesh generation is performed in ANSYS software, and periodic boundary conditions [9, 10] are applied for homogenization to derive linear elastic parameters. Then, the above linear elastic parameters are used as input to establish the meso-scale model, which is then homogenized [11, 12] to derive the macro-linear elastic parameters. The fiber matrix material parameters take the parameters in the literature [13] as input, as shown in Table I. The micro-scale model parameters are shown in Table II ($V_{ft1}$ is the fiber volume fraction in the micro RVE model), and the micro RVE model is shown in Fig 1.

**TABLE I. Material properties of the constituents**

| Material property | Fiber(T300) | Matrix(Epoxy resin) |
|---|---|---|
| $E_1$ (GPa) | 230 | 3.50 |
| $E_2$=$E_3$ (GPa) | 40 | |
| $G_{12}$=$G_{13}$ (GPa) | 24 | 1.30 |
| $G_{23}$ (GPa) | 14.30 | |
| $v_{12}$=$v_{13}$ | 0.26 | 0.35 |
| $v_{23}$ | 0.44 | |

**TABLE II. Microscopic RVE model parameters**

| Model property | Value |
|---|---|
| Fiber volume fraction in microscopic RVE model $V_{ft1}$ | 0.628 |
| Fiber diameter $d$ (μm) | 8.32 |
| microscopic RVE model length $L$ (mm) | 1 |
| microscopic RVE model width $W$ (mm) | 1 |
| microscopic RVE model thickness $H$ (mm) | $\sqrt{3}$ |

In order to verify whether the elastic parameters derived from micro-homogenization calculation are accurate, Chamis [14] model formula is used as the basis for judgment. The

*Forest Chemicals Revew*
*www.forestchemicalsreview.com*
*ISSN: 1520-0191*
*July-August 2021 Page No. 1469-1482*
*Article History: Received: 12 May 2021 Revised: 25 June 2021 Accepted: 22 July 2021 Publication: 31 August 2021*

Chamis model formula is shown in formulas 1~5:

$$E_{11} = V_f E_{11}^f + V_m E^m \tag{1}$$

$$E_{22} = E_{33} = \frac{E^m}{1 - \sqrt{V_f}\ (1 - E^m / E_{22}^f)} \tag{2}$$

$$G_{12} = G_{13} = \frac{G^m}{1 - \sqrt{V_f}\ (1 - G^m / G_{12}^f)} \tag{3}$$

$$G_{23} = \frac{G^m}{1 - \sqrt{V_f}\ (1 - G^m / G_{23}^f)} \tag{4}$$

$$v_{12} = V_f v_{12}^f + V_m v^m \tag{5}$$

Chamis model formula calculation is compared with micro-homogenization calculation, with the results shown in Table III. It can be seen that the micro-homogenization calculation results have an axial elastic modulus error of 0.01%, an axial Poisson's ratio error of 3.33%, while other parameters have bigger error, mainly because Chamis model does not consider the possible effect of different fiber arrangements on the transverse elastic modulus and shear modulus of the composite. This verifies the correctness of the micro-homogenization method.

**TABLE III. Microscopic RVE model calculation results**

| Material property | Chamis model | Homogenization | Error(%) |
|---|---|---|---|
| $E_1$ (GPa) | 145.74 | 145.75 | 0.01 |
| $E_2$=$E_3$ (GPa) | 12.64 | 11.70 | 7.44 |
| $G_{12}$=$G_{13}$ (GPa) | 5.19 | 4.68 | 9.83 |
| $G_{23}$ (GPa) | 4.65 | 4.07 | 12.47 |
| $v_{12}$=$v_{13}$ | 0.30 | 0.29 | 3.33 |
| $v_{23}$ | 0.36 | 0.45 | 25.05 |

*Forest Chemicals Revew*
*www.forestchemicalsreview.com*
*ISSN: 1520-0191*
*July-August 2021 Page No. 1469-1482*
*Article History: Received: 12 May 2021 Revised: 25 June 2021 Accepted: 22 July 2021 Publication: 31 August 2021*

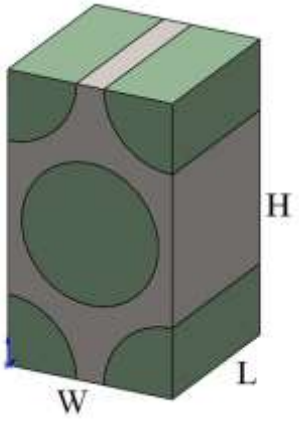


Fig 1: microscopic RVE model

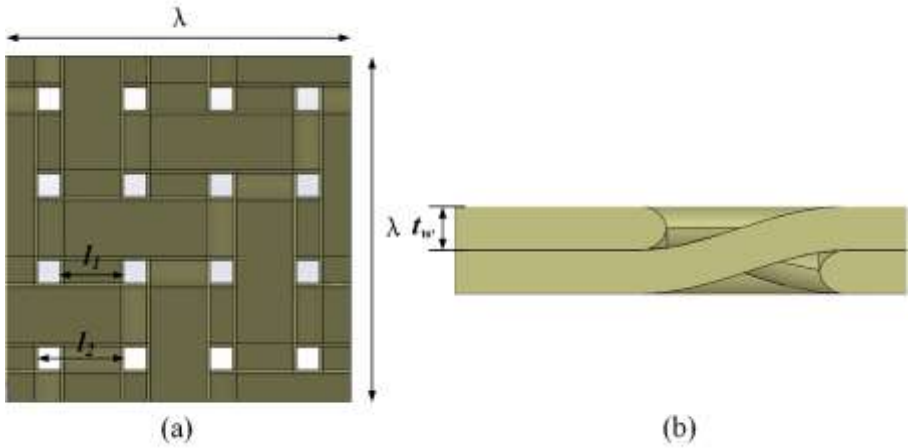


Fig 2: meso-scale RVE model: (a) 3D meso-scale RVE model, and (b) cross-section view of interlacing yarns

The parameters of the meso-scale model are shown in Table IV, and the mesoscopic RVE model is shown in Fig 2 (a, b). We usually think that braided composites are balanced. That is to say, the warp and weft have the same waviness and yarn volume fraction. Suppose that the adjacent yarns are filled with matrix, then yarn path can be described using a series of approximately rectangular cross-sectional strip shape, as shown in Fig 2(b). According to the yarn geometric parameters in Table II and Table III and the fiber volume fraction $V_{ft1}$ (equal to the fiber volume fraction $V_{ft2}$ in the yarn) in the microscopic RVE, the volume fraction $V_{tow}$ and fiber volume fraction $V_{fiber}$ of the yarn in the mesoscopic RVE are calculated using equations (6) and (7) (the fiber volume fraction is the volume fraction of fibers in the mesoscopic RVE, which is also approximately equal to the overall fiber volume fraction of the composite):

*Forest Chemicals Revew*
*www.forestchemicalsreview.com*
*ISSN: 1520-0191*
*July-August 2021 Page No. 1469-1482*
*Article History: Received: 12 May 2021 Revised: 25 June 2021 Accepted: 22 July 2021 Publication: 31 August 2021*

$$V_{tow} = \frac{8 \cdot l_1 t_w \lambda}{\lambda^2 \cdot 2t_w} \quad (6)$$

$$V_{fiber} = V_{tow} \cdot V_{ft2} \quad (7)$$

**TABLE IV. Meso-scale RVE model parameters**

| Model property | Value |
|---|---|
| Yarn width $l_1$ (mm) | 1.047 |
| Yarn spacing $l_2$ (mm) | 1.45 |
| Yarn thickness $t_w$ (mm) | 0.11 |
| Meso-scale RVE model width $\lambda$ (mm) | 5.80 |
| Yarn volume fraction $V_{tow}$ | 0.722 |
| Fiber volume fraction in yarn $V_{ft2}$ | 0.628 |
| Fiber volume fraction in weave $V_{fiber}$ | 0.453 |

The linear elastic results and material strength parameters calculated by the meso-scale model are shown in Table V:

**TABLE V. Meso-scale RVE model calculation results and strength parameters of the constituents**

| Material property | Homogenization | Strength property | Value |
|---|---|---|---|
| $E_1$= $E_2$ (GPa) | 49.26 | $S_{tx}$=$S_{ty}$ (MPa) | 693 |
| $E_3$ (GPa) | 10.36 | $S_{tz}$ (MPa) | 50 |
| $G_{12}$ (GPa) | 3.24 | $S_{cx}$=$S_{cy}$ (MPa) | -509 |
| $G_{13}$=$G_{23}$ (GPa) | 3.09 | $S_{cz}$ (MPa) | -107 |
| $\nu_{12}$ | 0.09 | $\tau_{yz}$=$\tau_{xz}$ (MPa) | 125 |
| $\nu_{13}$=$\nu_{23}$ | 0.43 | $\tau_{xy}$ (MPa) | 65 |

2.1.2 Macro-scale modeling

According to the standard specimen in reference [13], a three-dimensional model of the standard specimen is established at the macro scale, and the linear elastic parameters calculated by the meso-scale model are used as the input of the material parameters for the ply design of

*Forest Chemicals Revew*
*www.forestchemicalsreview.com*
*ISSN: 1520-0191*
*July-August 2021 Page No. 1469-1482*
*Article History: Received: 12 May 2021 Revised: 25 June 2021 Accepted: 22 July 2021 Publication: 31 August 2021*

the standard specimen. The macroscopic model of standard specimen is finally obtained (each layer thickness is 0.23mm, the ply parameter is $[0^o]_9$). Fig 3 shows a schematic diagram of the standard specimen.

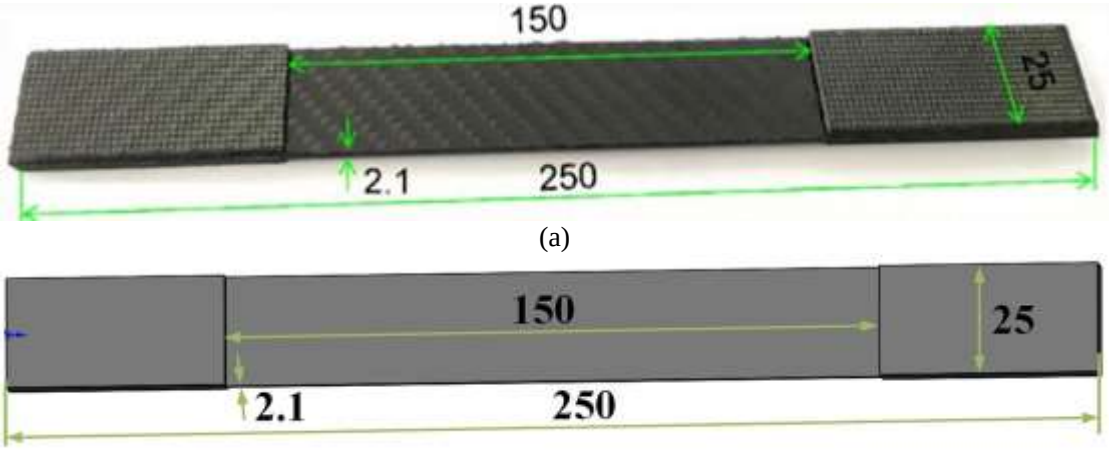


Fig 3: schematic diagram of standard specimens of carbon fiber composites: (a) physical of standard specimen, and (b) Standard specimen 3D model

The predicted value of the multi-scale high-fidelity digital model established herein and the three experimental data stress-strain curves in the literature [13] are shown in Fig 4. The MFE curve is the predicted data of the multi-scale high-fidelity digital model, and EXP1, EXP2, and EXP3 are respectively the three experimental data curves in the literature [13]. From Fig 4, it can be seen that the material elastic modulus predicted by the multi-scale high-fidelity digital model after fiber and matrix damage initiation is slightly higher than the experimental value. Compared with the three test curves in literature [13], The stress-strain curve errors predicted by the multi-scale high-fidelity digital model established in this paper are 6.41%, 10.16%, 13.20% respectively, and the average error is 9.92% < 10%, which proves the correctness of the multi-scale high-fidelity digital model.

*Forest Chemicals Revew*
*www.forestchemicalsreview.com*
*ISSN: 1520-0191*
*July-August 2021 Page No. 1469-1482*
*Article History: Received: 12 May 2021 Revised: 25 June 2021 Accepted: 22 July 2021 Publication: 31 August 2021*

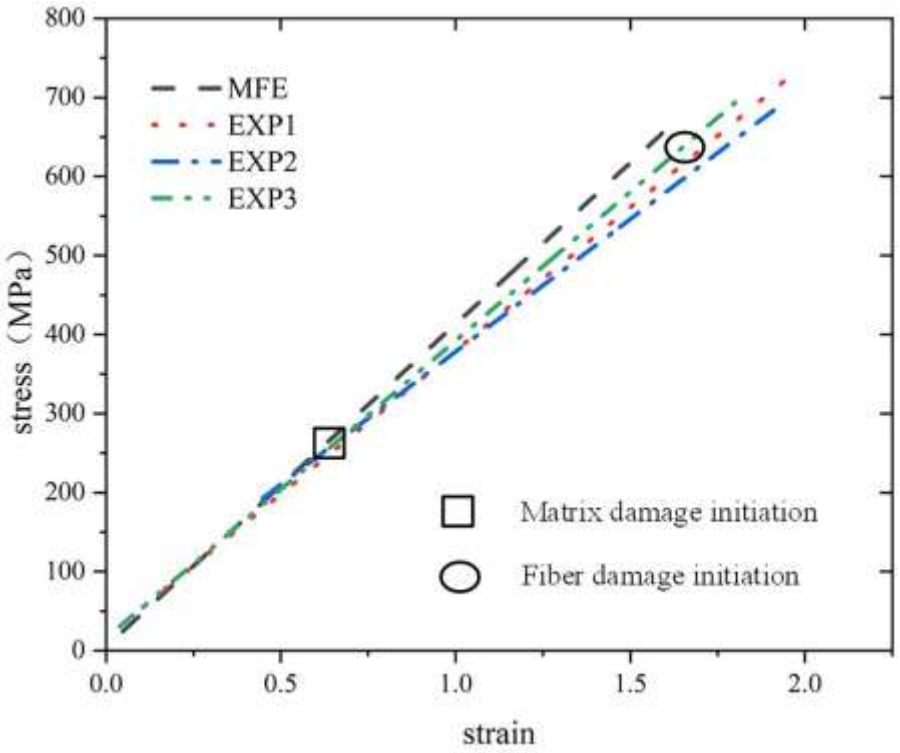


Fig 4: comparison between multiscale finite element model prediction and testing and tested stress-strain curves

2.2 Reduced-order Model

Reduced-order model is derived based on the training data of the BP neural network model. The process for establishing the BP neural network reduced-order model can be divided into four steps: collecting data, creating a configuration network, training the network, verifying and using the network.

2.2.1 Collect data

The reduced-order model is aimed at the stretching process of two-dimensional braided twill composites. Considering the needs of digital twin, the input variables in the data set are node coordinate data and node load data, and the output data are node stress and strain data. Some data of the neural network training set are shown in Table VI.

**TABLE VI. Neural network partial training set data**

| **Input data** | **Output data** |
|---|---|

*Forest Chemicals Revew*
*www.forestchemicalsreview.com*
*ISSN: 1520-0191*
*July-August 2021 Page No. 1469-1482*
*Article History: Received: 12 May 2021 Revised: 25 June 2021 Accepted: 22 July 2021 Publication: 31 August 2021*

| x (mm) | y (mm) | F (N) | Stress (MPa) | Strain |
|---|---|---|---|---|
| 246.03 | 12.50 | 10291 | 167.25 | 0.40 |
| 246.03 | 12.50 | 15405 | 265.37 | 0.64 |
| 246.03 | 12.50 | 20499 | 363.29 | 0.88 |
| 246.03 | 12.50 | 25572 | 461.03 | 1.12 |
| 246.03 | 12.50 | 30625 | 558.57 | 1.35 |
| 246.03 | 12.50 | 31482 | 603.70 | 1.46 |
| 246.03 | 12.50 | 31885 | 611.48 | 1.48 |
| 246.03 | 12.50 | 32321 | 619.92 | 1.50 |
| 246.03 | 12.50 | 32724 | 627.70 | 1.52 |
| 246.03 | 12.50 | 33160 | 636.14 | 1.54 |
| 246.03 | 12.50 | 33563 | 643.92 | 1.56 |
| 246.03 | 12.50 | 33998 | 652.34 | 1.58 |
| 246.03 | 12.50 | 34398 | 660.10 | 1.60 |
| 246.03 | 12.50 | 34833 | 668.49 | 1.62 |
| 246.03 | 12.50 | 33400 | 657.84 | 1.59 |
| 246.03 | 12.50 | 30522 | 585.24 | 1.42 |

2.2.2 Create and configure network

Create a BP neural network model, which is a feed forward neural network model composed of input layer, hidden layer, and output layer. First, enter the data volume ratio of the training set, validation set, and test set, and then enter the number of hidden layer neurons to complete the network configuration. The ratio used in this model is 70%: 15%: 15%, and the number of neurons is 10. Feed forward networks usually have one or more hidden layers composed of neurons, followed by an output layer composed of linear neurons. A multi-layer composed of neurons with a non-linear transfer function allows the network to learn the non-linear relationship between input and output variables. The linear output layer is most commonly used for function fitting (or nonlinear regression) problems.

2.2.3 Train the network

There are three commonly used training algorithms in BP neural network training: B-R [15], L-M [16], SCG [17]. Where, B-R expresses its parameters in probability distribution to provide uncertainty estimation. The algorithm has longer calculation time, but its calculation is more accurate. L-M is the most widely used nonlinear least squares algorithm which uses gradients to solve the maximum (minimum) value. When calculating with a computer, the algorithm occupies much memory and supports fast calculation. SCG is a method between the steepest

*Forest Chemicals Revew*
*www.forestchemicalsreview.com*
*ISSN: 1520-0191*
*July-August 2021 Page No. 1469-1482*
*Article History: Received: 12 May 2021 Revised: 25 June 2021 Accepted: 22 July 2021 Publication: 31 August 2021*

descent method and the Newton method, which only needs the first derivative information. Its advantages include small storage amount, step convergence, and high stability, but its calculation accuracy is relatively poor. Table VII shows the prediction data of the three algorithms and the multi-scale high-fidelity digital model data.

**TABLE VII. Three algorithms for response data**

| Stress (MPa) | | | | | Strain | | | | |
|---|---|---|---|---|---|---|---|---|---|
| **Time** | **B-R** | **L-M** | **SCG** | **MFE** | **Time** | **B-R** | **L-M** | **SCG** | **MFE** |
| 60.0 | 66.88 | 70.48 | 81.86 | 98.51 | 60.0 | 0.17 | 0.92 | -3.65 | 0.24 |
| 120.0 | 165.03 | 165.12 | 166.72 | 196.81 | 120.0 | 0.41 | 0.80 | -3.01 | 0.48 |
| 180.0 | 265.09 | 264.57 | 250.13 | 294.93 | 180.0 | 0.65 | 0.71 | -1.70 | 0.71 |
| 240.0 | 363.04 | 361.46 | 355.67 | 392.85 | 240.0 | 0.89 | 0.74 | -0.14 | 0.95 |
| 300.0 | 461.79 | 455.34 | 454.08 | 461.27 | 300.0 | 1.13 | 0.98 | 0.65 | 1.12 |
| 360.0 | 576.75 | 574.69 | 575.34 | 588.10 | 360.0 | 1.45 | 1.39 | 1.07 | 1.42 |
| 370.2 | 596.51 | 598.82 | 597.57 | 604.67 | 370.2 | 1.50 | 1.50 | 1.13 | 1.46 |
| 375.0 | 606.56 | 609.72 | 607.61 | 612.46 | 375.0 | 1.52 | 1.55 | 1.16 | 1.48 |
| 380.2 | 620.38 | 620.95 | 618.04 | 620.90 | 380.2 | 1.54 | 1.60 | 1.19 | 1.50 |
| 385.0 | 636.92 | 630.73 | 627.21 | 628.69 | 385.0 | 1.55 | 1.64 | 1.22 | 1.52 |
| 390.2 | 647.79 | 640.58 | 636.56 | 637.12 | 390.2 | 1.56 | 1.69 | 1.25 | 1.54 |
| 395.0 | 650.14 | 649.01 | 644.63 | 644.91 | 395.0 | 1.58 | 1.73 | 1.27 | 1.56 |
| 400.2 | 655.01 | 657.42 | 652.71 | 653.36 | 400.2 | 1.60 | 1.77 | 1.29 | 1.58 |
| 405.0 | 661.05 | 664.58 | 659.53 | 661.15 | 405.0 | 1.62 | 1.80 | 1.31 | 1.60 |
| 410.2 | 667.77 | 671.80 | 666.30 | 669.45 | 410.2 | 1.63 | 1.84 | 1.33 | 1.62 |
| 415.0 | 649.19 | 645.68 | 641.44 | 710.24 | 415.0 | 1.57 | 1.71 | 1.26 | 1.73 |
| 417.8 | 574.37 | 571.76 | 572.61 | 587.79 | 417.8 | 1.44 | 1.38 | 1.06 | 2.21 |

Fig 5(a) shows the strain error curves of the predicted values of the three algorithms and the multi-scale high-fidelity digital model. Fig 5(a) shows the stress error curve of the predicted values of the three algorithms and the multi-scale high-fidelity digital model. For strain prediction, B-R demonstrates obvious advantages, and the three algorithms have similar prediction accuracy in stress prediction. The average error of the three algorithms in predicting stress and strain is shown in Table VIII. Considering the stress and strain, the average error of the stress and strain predicted by B-R is 5.03% and 7.19% respectively. Therefore, it is appropriate to use the B-R training data to establish a neural network reduced-order model.

*Forest Chemicals Revew*
*www.forestchemicalsreview.com*
*ISSN: 1520-0191*
*July-August 2021 Page No. 1469-1482*
*Article History: Received: 12 May 2021 Revised: 25 June 2021 Accepted: 22 July 2021 Publication: 31 August 2021*

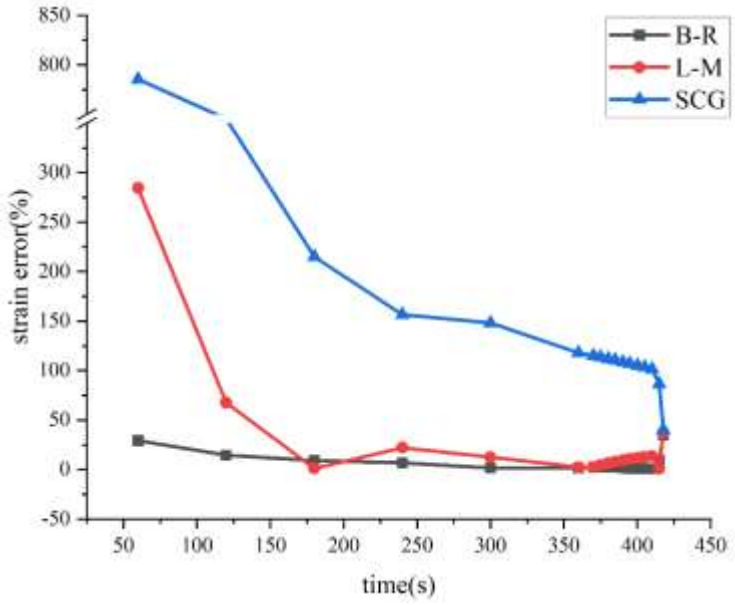


(a)

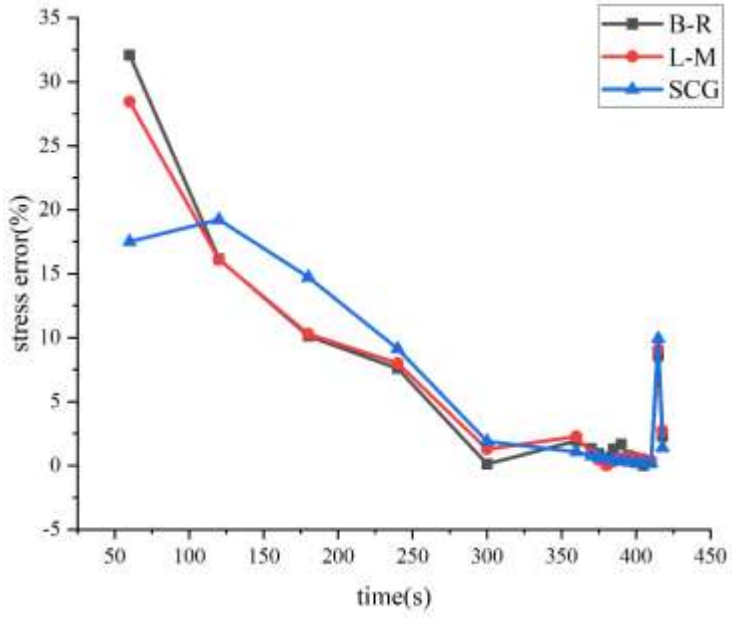


(b)

Fig 5: three algorithm response data error curves: (a) strain error curves, and (b) stress error curves

**TABLE VIII. Average error of response data for three algorithms**

*Forest Chemicals Revew*
*www.forestchemicalsreview.com*
*ISSN: 1520-0191*
*July-August 2021 Page No. 1469-1482*
*Article History: Received: 12 May 2021 Revised: 25 June 2021 Accepted: 22 July 2021 Publication: 31 August 2021*

| Algorithm properties | B-R | L-M | SCG |
|---|---|---|---|
| Average error of stress prediction data | 5.03 | 4.86 | 4.62 |
| Average error of strain prediction data | 7.19 | 29.92 | 169.59 |

2.2.4 Verify and use the network

The stress-strain curves predicted by the neural network reduced-order model and the multi-scale high-fidelity digital model established herein are shown in Fig 6. The MFE curve shows the prediction data of the multi-scale high-fidelity digital model, and the NET curve shows the prediction data of neural network reduced-order model. The predicted value of the established neural network reduced-order model and multi-scale high-fidelity digital model has the maximum error when the strain is 1.77%, the maximum error is 5.64%, indicating that the neural network reduced-order model established by the B-R training data has sufficient prediction accuracy.

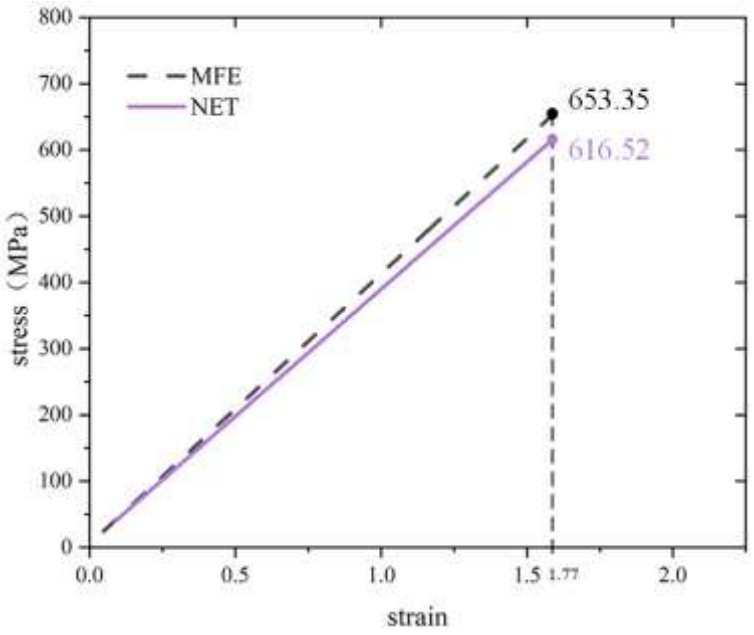


Fig 6: comparison between multiscale finite element model predicted and reduced order model predicted stress-strain curves

## III. CONCLUSION

This paper investigates multi-scale modeling and neural network reduced-order model of the composite structure, and the following conclusions are drawn:

*Forest Chemicals Revew*
*www.forestchemicalsreview.com*
*ISSN: 1520-0191*
*July-August 2021 Page No. 1469-1482*
*Article History: Received: 12 May 2021 Revised: 25 June 2021 Accepted: 22 July 2021 Publication: 31 August 2021*

In the multi-scale modeling of composite structure, compared with the theoretical model calculation, multi-scale model homogenization calculation result has higher calculation accuracy for axial elastic modulus, and the prediction error of other elastic parameters is also within a reasonable range.

Seen from the perspective of macro stress-strain curve, the initial stiffness predicted by the multi-scale high-fidelity digital model and the neural network reduced-order model is in good agreement with the experimental value. When the matrix has initial damage and the structure exhibits severe nonlinearity, the prediction data of the multi-scale high-fidelity digital model and the neural network reduced-order model deviates from the real test data. The maximum error between the prediction data and the experimental data of the multi-scale high-fidelity digital model is 13.20%, and the average error of the three experiments is 9.92%, indicating that the digital model can accurately describe the composite structure and meet the requirements for digital twin modeling of composite structures.

The maximum error in predicted data between the neural network reduced-order model and the multi-scale high-fidelity digital model is 5.64%. The reduced-order model enables sufficient data accuracy under the premise of real-time data prediction of digital twin modeling.

## REFERENCES

[1] Jiao W, Chen L, Xie J, et al. (2020) Effect of weaving structures on the geometry variations and mechanical properties of 3D LTL woven composites. Composite Structures, 252: 112756
[2] Dai S, Cunningham P R (2016) Multi-scale damage modelling of 3D woven composites under uni-axial tension. Composite Structures, 142: 298–312
[3] Tuegel EJ, Ingraffea AR, Eason TG, et al. (2011) Reengineering Aircraft Structural Life Prediction Using a Digital Twin. International Journal of Aerospace Engineering, 2011: e154798
[4] Lai X, Wang S, Guo Z, et al. (2021) Designing a Shape-Performance Integrated Digital Twin Based on Multiple Models and Dynamic Data: A Boom Crane Example. Journal of Mechanical Design, 143(7): 071703
[5] Botz M, Emiroglu A, Osterminski K, et al. (2020) Monitoring and Modeling of a Wind Turbine Support Structure to Create a Digital Twin. Beton- Und Stahlbetonbau, 115(5): 342–354
[6] Saboktakin A, Kalaoglu F, Shahrooz M (2021) Multiscale Analysis of Damage Progression in Reinforced Textile Composite. Journal of Inorganic and Organometallic Polymers and Materials, 31(1): 55–61
[7] Han X, Xu C, Xie W, et al. (2019) Multiscale computational homogenization of woven composites from microscale to mesoscale using data-driven self-consistent clustering analysis. Composite Structures, 220: 760–768
[8] Wu L, Adam L, Noels L (2021) Micro-mechanics and data-driven based reduced order models for multi-scale analyses of woven composites. Composite Structures, 270: 114058

*Forest Chemicals Revew*
*www.forestchemicalsreview.com*
*ISSN: 1520-0191*
*July-August 2021 Page No. 1469-1482*
*Article History: Received: 12 May 2021 Revised: 25 June 2021 Accepted: 22 July 2021 Publication: 31 August 2021*

[9] Benveniste Y. (1987) A new approach to the application of Mori-Tanaka's theory in composite materials. Mechanics of Materials, 6(2): 147–157

[10] Parnell WJ. (2016) The Eshelby, Hill, Moment and Concentration Tensors for Ellipsoidal Inhomogeneities in the Newtonian Potential Problem and Linear Elastostatics. Journal of Elasticity, 125(2): 231–294

[11] Li S, Jeanmeure LFC, Pan Q (2015) A composite material characterisation tool: UnitCells. Journal of Engineering Mathematics, 95(1): 279–293

[12] Li S (2008) Boundary conditions for unit cells from periodic microstructures and their implications. Composites Science and Technology, 68(9): 1962–1974

[13] Wang L, Wu J, Chen C, et al. (2017) Progressive failure analysis of 2D woven composites at the meso-micro scale. Composite Structures, 178: 395–405

[14] Chamis CC (1989) Mechanics of Composite Materials: Past, Present, and Future. Journal of Composites, Technology and Research, 11(1): 3–14

[15] MacKay DJC. (1992) Bayesian Interpolation. Neural Computation, 4(3): 415–447

[16] Marquardt DW (2006) An Algorithm for Least-Squares Estimation of Nonlinear Parameters. Journal of the Society for Industrial and Applied Mathematics

[17] Møller MF. (1993) A scaled conjugate gradient algorithm for fast supervised learning. Neural Networks, 6(4): 525–533